Scatterings and Quantum Effects in (Al,In)N/GaN Heterostructures for High-Power and High-Frequency Electronics

Leizhi Wang,[1] Ming Yin,[2] Asif Khan,[3] Sakib Muhtadi,[3] Fatima Asif,[3] Eun Sang Choi,[4] and Timir Datta[1,*]

[1]*Department of Physics and Astronomy, University of South Carolina, Columbia, South Carolina 29208, USA*

[2]*Department of Physics and Engineering, Benedict College, Columbia, South Carolina 29204, USA*

[3]*Department of Electrical Engineering, University of South Carolina, Columbia, South Carolina 29208, USA*

[4]*National High Magnetic Field Laboratory, Tallahassee, Florida 32310, USA*

(Received 30 December 2016; revised manuscript received 26 July 2017; published 7 February 2018)

Charge transport in the wide-band-gap (Al, In)N/GaN heterostructures with high carrier density approximately 2×10^{13} cm^{-2} is investigated over a large range of temperature (270 mK $\leq T \leq$ 280 K) and magnetic field ($0 \leq B \leq 18$ T). We observe the first evidence of weak localization in the two-dimensional electron gas in this system. From the Shubnikov–de Haas (SdH) oscillations a relatively light effective mass of $0.23m_e$ is determined. Furthermore, the linear dependence with temperature ($T < 20$ K) of the inelastic scattering rate ($\tau_i^{-1} \propto T$) is attributed to the phase breaking by electron-electron scattering. Also in the same temperature range the less-than unit ratio of quantum lifetime to Hall transport time ($\tau_q/\tau_t < 1$) is taken to signify the dominance of small-angle scattering. Above 20 K, with increasing temperature scattering changes from acoustic phonon to optical phonon scattering, resulting in a rapid decrease in carrier mobility and increase in sheet resistance. Suppression of such scatterings will lead to higher mobility and a way forward to high-power and high-frequency electronics.

DOI: 10.1103/PhysRevApplied.9.024006

I. INTRODUCTION

Presently, there is a demand for dramatic improvements in energy usage, and devices that control large amounts of electrical energy, rapidly with minimal loss. The need for reliable, faster, smaller, and high efficiency but cheaper power devices is also urgent. However, Si-based power technology already operates nearly at the theoretical upper bound. Hence, new electronic materials with high off-state blocking voltage and on-state conductance are in demand. The wide-band-gap III–V semiconductors are such materials. Of the wide-band-gap nitrides, GaN is particularly attractive, because the two-dimensional electron gas (2DEG) in GaN heterostructures arises from the polarization-induced surface charge distribution, without chemical doping; the absence of impurity (dopant) atoms decreases scattering and improves charge conduction. The barrier layer material is also critical in improving crystal quality, carrier mobility, and performance. For instance, the choice of indium in the (Al, In)N/GaN configuration allows tuning of the AlN and InN composition [1–3] leading to better lattice matching to GaN. Plus due to its larger spontaneous polarization [4,5], carrier density in the (Al, In)N/GaN may reach three times higher than similar (Al,Ga)N-based structures [1]. Additionally, the wider band gap and high thermal and chemical stabilities of (Al,In)N may allow device operation above 1000 °C [4]. Overall, the (Al, In)N/GaN configuration is well suited for high-power and high-frequency electronics.

To realize the desired performance goals, along with the search for new wide-band-gap and high-carrier-density materials, it is also important to understand the physical processes, especially mechanisms that limit mobility in the device structure. Transport measurements are effective tools for studying scattering process and can provide valuable information about the material including Fermi surface, effective mass, quantum dephasing, and relaxation times [5–9]. These parameters have been extensively investigated in (Al, Ga)N/GaN structures. However, behaviors in this new (Al, In)N/GaN system have not yet been widely reported. In this article, we report on the classical as well as quantum-transport properties of high-carrier-density around 2×10^{13} cm^{-2} 2DEG in (Al, In)N/GaN heterostructures, over a large region of the temperature (270 mK $\leq T \leq$ 280 K) and magnetic field ($0 \leq B \leq 18$ T) phase space.

Quantum interference and coherent back scattering leads to weak localization [5,10–12] that is evidenced by an increased resistance above the classical Drude value. The

*Corresponding author.
datta@sc.edu

application of a magnetic field breaks the time-reversal symmetry and shifts or destroys the conditions for constructive interference. Hence, localization probability is decreased with an increasing magnetic field leading to a counterintuitive increase in the magnetoconductivity. Important material parameters such as elastic scattering time and the inelastic phase-breaking time can be readily obtained from such quantum- transport measurements [11,13].

At high magnetic fields, the carriers in the interior region of the material execute cyclotron motion. But Landau motion is disrupted by the boundaries; the carriers get scattered forward along the edge, leading to a "superhigh current" that adds to the current flow and increases conductance. With increasing magnetic field the system traverses through the quantized Landau levels, and the resistance oscillates periodically as a function of $1/B$, a behavior known as Shubnikov–de Haas (SdH) oscillation [7,9,14,15]. SdH is useful to investigate the quantum scattering mechanism and analyze materials' properties including effective mass.

From the SdH signal and Dingle plot, we determine the quantum lifetime and the electron effective mass. At high temperatures ($T > 20$ K) thermal effects suppress both weak localization and SdH oscillations. Also in this regime, with the increasing temperature scattering changes from acoustic phonon to optical phonon scattering. The control of scattering in $(\mathrm{Al,In})\mathrm{N}/\mathrm{GaN}$ heterostructures will be essential for practical applications.

II. EXPERIMENT

The $Al_{0.83}In_{0.17}N/GaN$ epilayer structures are grown on sapphire substrates by the standard metal-organic chemical vapor deposition process [16]. Figure 1(a) is a scanning-electron-microscope (SEM) image of the cross-sectional view of a heterostructure. It clearly shows a roughly 200 nm AlN buffer layer followed by 2.2 μm undoped GaN as channel layer, around 1 nm AlN spacer and 7 nm (Al,In)N barrier layer with In composition of 17%. The 1 nm AlN spacer is deposited before (Al,In)N growth, which effectively confines the electron gas in the quantum well and reduces the alloy scattering [2]. The Hall bar mesas are defined by photolithography and followed by an inductively coupled plasma etching using Cl_2/BCl_3, as shown in the schematic diagram of Fig. 1(b). Six Ohmic contacts are formed by evaporating Ti (40 nm thick), Al (120 nm), Ti (40 nm), and Au (80 nm) films in sequence using e-beam deposition and then annealing at 850 °C for 30 sec in N_2 ambient in order to diffuse Al to the 2DEG region. The low-frequency (17.97 Hz) phase sensitive

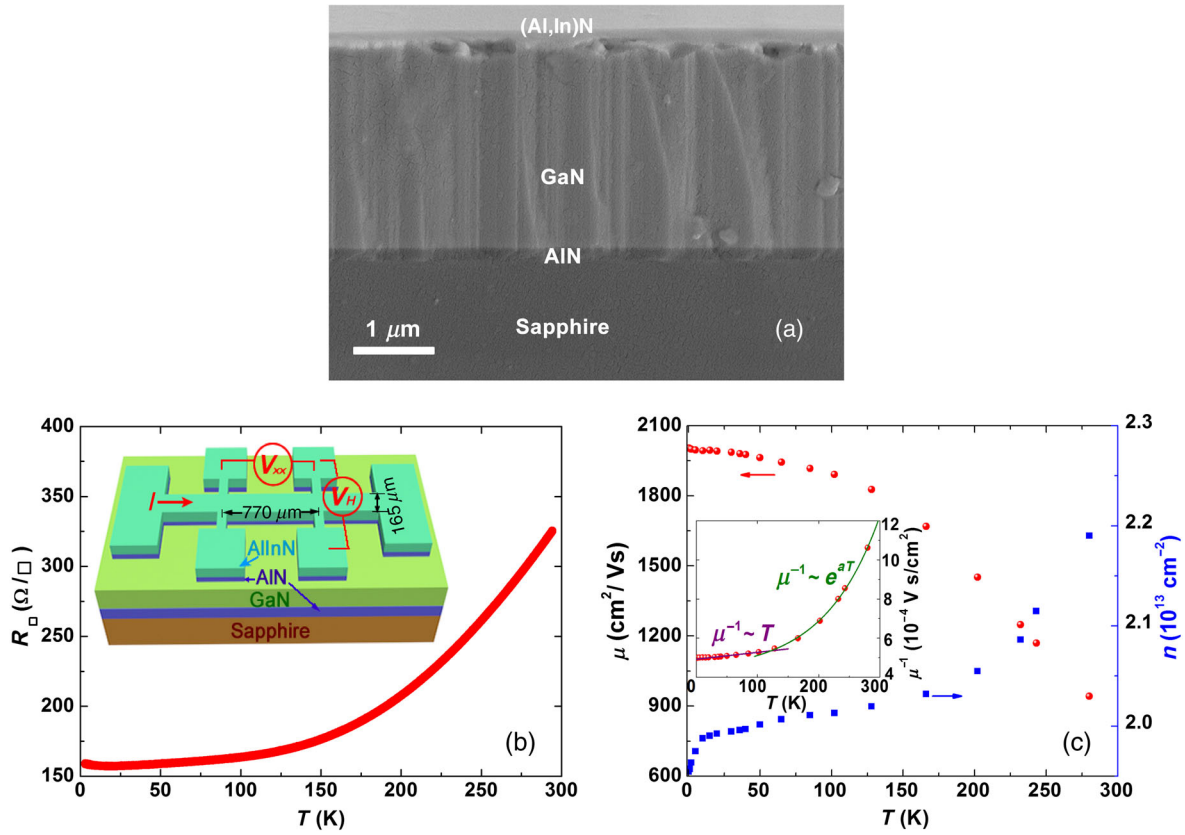

FIG. 1. (a) Cross-section SEM image of $(\mathrm{Al,In})\mathrm{N}/\mathrm{GaN}$ heterostructure. (b) Temperature-dependent sheet resistance, inset is the schematic diagram of structure. (c) Carrier density and Hall mobility as a function of temperature.

transport measurements are conducted, with an applied current of 1 μA using a SR830 DSP lock-in amplifier, in an 18/20 Tesla Superconducting Magnet (SCM2) with a ^{3}He insert of the NHMFL.

III. RESULTS AND DISCUSSION

A. Temperature-dependent electrical transport

The typical temperature dependence of sheet resistance, $R_\square$ is shown in Fig. 1(b). As will be clear above 20 K, the behavior is consistent with metalliclike transport; $R_\square$ generally increases with increasing temperature. The variation of the Hall carrier density as a function of temperature is shown in Fig. 1(c). Although the density increases with increasing temperature, the change is very small. This is because of the large band gap: $E_g \approx 4$ eV [17,18]. In the regime of interest (270 mK $\sim$ 280 K), $k_BT \ll E_g$ and the carrier density remains nearly temperature independent.

In contrast, the Hall mobility falls with an increasing temperature, and the decreasing rate exhibits an interesting variation with temperature. Below 20 K, the mobility is weakly temperature dependent, mirroring that of the sheet resistance. As will be discussed later, these behaviors may arise from impurity scattering or surface roughness as well as electron-electron scattering. As shown in the inset of Fig. 1(c), between 20 and 100 K, the temperature dependence is more pronounced and inverse mobility is directly proportional to temperature, $\mu^{-1} \propto T$, indicating that acoustic phonon scattering is dominant [2,19,20]. Such temperature dependence is also observed in (Al, Ga)N/GaN structures. At higher temperatures, above 100 K, mobility decreases even faster and an exponential dependence $\mu \propto e^{-aT}$ describes the data very well. In the 2DEG literature, such exponential $\mu(T)$ at high temperatures has been attributed to polar optical phonon scattering [2,21]. Quite generally, throughout the measured temperature range the mobility is reduced with increasing temperature.

B. Shubnikov–de Haas oscillation

The longitudinal resistance R_{xx} isotherm as a function of applied magnetic field B up to 18 T is shown in Fig. 2(a). As the magnetic field is increased, Shubnikov–de Haas (SdH) oscillations appear. The peaks of the oscillations are pronounced at low temperatures and damped with increasing temperature. This effect is more apparent in ΔR_{xx} after subtracting the background from R_{xx} [Fig. 2(b)]. SdH oscillations are a periodic function of $1/B$. Evidence of multiple subbands in (Al, In)N/GaN or (Al, Ga)N/GaN heterostructures has been reported [5,22]. However, Fourier transform (FT) analysis of ΔR_{xx} for our data results in a single peak frequency $B_F = 403$ T, as shown in the inset of Fig. 2(b). This indicates that only one band is dominant in our sample. Also, the frequency B_F is directly related to the carrier density by $n_{\mathrm{SdH}} = 2eB_F/h$. Hence, the carrier density of this sample is $n_{\mathrm{SdH}} = 1.95 \times 10^{13}$ cm^{-2}. This agrees very well with the averaged value obtained from Hall measurement.

The amplitude of the SdH oscillation is given by [8,14] $\Delta R_{xx} = 4R_0[\chi/(\sinh\chi)]\exp[(-\pi)/(\omega_c\tau_q)]$. Here, τ_q is the quantum lifetime, $\chi = 2\pi^2 k_B T/\Delta E$ and the Landau-level energy gap is $\Delta E = \hbar\omega_c = \hbar eB/m^*$; k_B is the Boltzmann constant, $\hbar$ is the reduced Planck constant, and e is the electron charge.

The effective mass of electrons m^* can be extracted from the temperature dependence of the SdH amplitude at a constant magnetic field by the following ratio [15]

$$\frac{\Delta R_{xx}(T,B)}{\Delta R_{xx}(T_0,B)} = \frac{T\sinh[\chi(T_0)]}{T_0\sinh[\chi(T)]} = \frac{T\sinh[2\pi^2 k_B T_0/\Delta E(B)]}{T_0\sinh[2\pi^2 k_B T/\Delta E(B)]}. \quad (1)$$

Here, we chose the lowest temperature 0.27 K as T_0. Figure 3(a) shows the above ratio of amplitude at $T_0 =$ 0.27 K and $B = 17.7$ T. Analyzing our data using Eq. (1) we

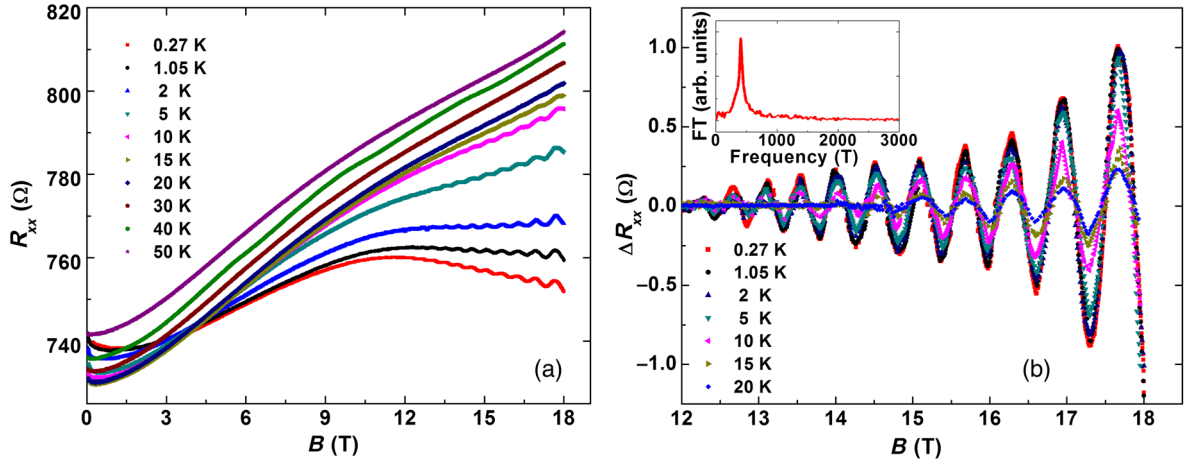

FIG. 2. (a) Magnetoresistance up to 18 T at a set of temperatures. (b) Shubnikov–de Haas oscillations after subtracting the background. Inset is Fourier transform (FT) amplitude as a function of frequency.

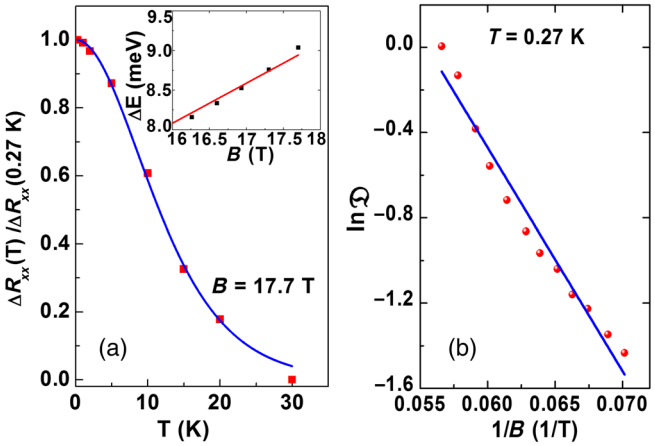

FIG. 3. (a) Effective mass plot at 17.7 T, where the data are best fit to Eq. (1); inset is field dependence of the Landau-level spacing. (b) Dingle plot to obtain the quantum lifetime in (Al, In)N/GaN heterostructure.

can extract $\Delta E(B)$. The inset of Fig. 3(a) shows the field dependence of the Landau-level energy gap. Thus, the corresponding effective mass is $m^* = 0.233m_e$, similar to the values reported in (Al, In)N/GaN heterostructures which are $0.22m_e$ and $0.25m_e$ [22,23] and in (Al, Ga)N/GaN systems which are $0.23m_e$ and $0.24m_e$ [24,25], respectively.

The quantum lifetime is obtained from the slope of the Dingle plot, as shown in Fig. 3(b), because

$$\ln \mathfrak{D} = \ln\left(\frac{\Delta R(T,B)\sinh[2\pi^2 k_B T/\Delta E(B)]}{2\pi^2 k_B T/\Delta E(B)}\right) = C_0 - \frac{\pi m^*}{e\tau_q B}, \tag{2}$$

where $\mathfrak{D}$ is the expression within the bracket, C_0 is a constant. In this sample the quantum lifetime is $\tau_q = 0.035$ ps. Furthermore, τ_q also determines the Dingle temperature $T_D = h/(4\pi^2 k_B \tau_q)$, which is a measure of the disorder. At $T = 0.27$ K, we find a relatively high value $T_D = 34.7$ K. Also, the broadening of the Landau levels [8,14], as determined by $k_B T_D \approx 3$ meV, is not much smaller than the Landau-level spacing $\Delta E(B) = 9.04$ meV at 17.7 T. This may explain the relatively small amplitude $\Delta R_{xx}/R_{xx} \ll 1$ of the SdH oscillations.

It is instructive to compare the quantum relaxation rate to transport rate, since $1/\tau_q = \int P(\theta)d\theta$ and $1/\tau_t = \int P(\theta)(1-\cos\theta)d\theta$, where $P(\theta)$ is the probability of scattering through an angle θ. The quantum lifetime τ_q includes information of all scatterings; however, the transport lifetime τ_t obtained from Hall mobility is weighted by the scattering angle and mainly determined by large-angle scattering [24,26,27]. Here, the transport lifetime $\tau_t = 0.252$ ps is nearly an order of magnitude larger than the quantum lifetime. In particular, the ratio $\tau_t/\tau_q = 7.2$ indicates that small-angle scattering associated with long-range interaction due to distant ionized impurities is the dominant scattering mechanism in our sample.

C. Weak localization

As is evident from Fig. 2(a), at low magnetic fields R_{xx} decreases with the applied field; that is, conductivity goes up with increasing field. This negative magnetoresistance arises from weak localization. It is convenient to define the magnetoconductivity by $\sigma_{xx} = \rho_{xx}/(\rho_{xx}^2 + \rho_{xy}^2)$. The quantum correction to the change in magnetoconductivity at low magnetic fields is [5,25,28,29]

$$\Delta\sigma_{xx} = \sigma_{xx}(B) - \sigma_{xx}(0) = \frac{e^2}{\pi h}\left[\psi\left(\frac{1}{2} + \frac{\hbar}{4eDB\tau_i}\right) - \psi\left(\frac{1}{2} + \frac{\hbar}{4eDB\tau_e}\right) + \ln\left(\frac{\tau_i}{\tau_e}\right)\right]. \tag{3}$$

Here, ψ is the digamma function; τ_i and τ_e are the inelastic and elastic scattering times, respectively; D is the diffusion constant given by $D = {v_F}^2\tau/2$, and for our two-dimensional system the Fermi velocity $v_F = \hbar k_F/m^* = \hbar\sqrt{2\pi n}/m^* = 0.5504 \times 10^6$ m/s. By choosing the parameter value estimated earlier $\tau \equiv \tau_t = 0.252$ ps, we determined $D = 0.0382$ m^2/s and the mean free path $l = v_F\tau_t = 139$ nm [7].

The inelastic and elastic scattering times are computed from the best-fit analysis of experimental data to Eq. (3). $\Delta\sigma_{xx}$ for a set of temperatures is shown in Fig. 4(a). For a constant temperature the conductivity increases with increasing magnetic field, and at higher temperature, the conductivity is reduced. We find that Eq. (3) describes the experimental data very well for temperatures below 20 K, which allows us to obtain the values of the relaxation times. Interestingly, the elastic scattering time τ_e is constant with temperature; this may be due to the short-range interactions such as impurity or interface roughness scatterings. Also, $\tau_e = 0.144$ ps is the same order as the transport time τ_t. However, the inelastic scattering time (phase coherence time) τ_i is much larger than the elastic scattering time and transport lifetime at low temperatures. This is necessary for the observation of weak localization, because the phase coherence length should be long enough so that the carrier can return to the origin after several scatterings. In addition, τ_i decreases with increasing temperature. In fact, the inelastic scattering rate is linearly proportional to temperature, $\tau_i^{-1} \propto T$, as shown in Fig. 4(b). This linearity has been attributed to phase breaking by inelastic electron-electron scattering [5,6].

The effect of electron-electron scattering is also observed in the absence of the magnetic field. As shown in the inset of Fig. 4(b), the sheet resistance at low temperatures is nonmonotonic. With increasing temperature it first decreases until 20 K and then increases. This

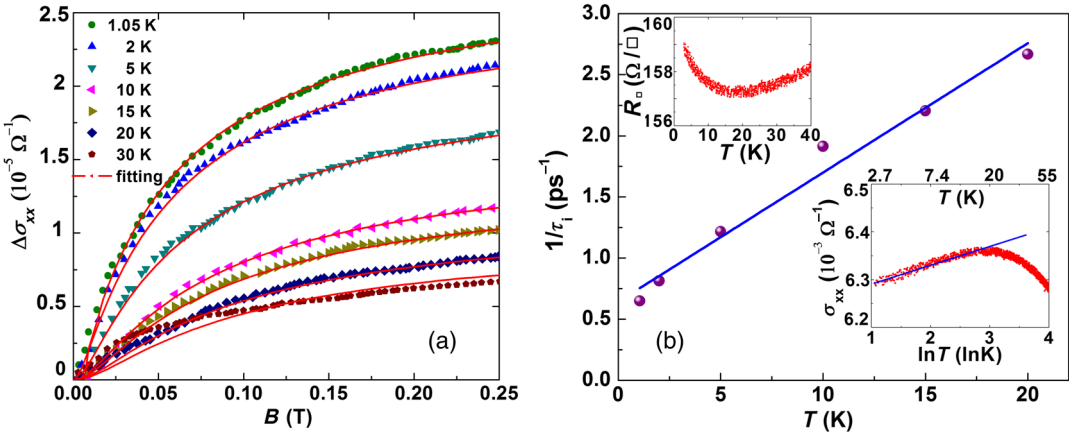

FIG. 4. (a) Magnetoconductivity at low magnetic fields for several temperatures. (b) The inelastic scattering rate displays linear temperature dependence. Insets are the zero-field resistance and conductivity, respectively.

enhanced conductivity for less than 20 K is also due to weak localization. Because the quantum interference correction at zero magnetic field is [28,30],

$$\sigma_{xx}(B=0) = \frac{e^2}{\pi h}\left[\psi\left(\frac{1}{2}+\frac{\hbar}{4eDB\tau_i}\right)-\psi\left(\frac{1}{2}+\frac{\hbar}{4eDB\tau_e}\right)\right] \cong -\frac{e^2}{\pi h}\ln\frac{\tau_i}{\tau_e}, \quad (4)$$

since $\psi(x) \to \ln x$ when $x \gg 1$.

As stated above, $\tau_i \propto T^{-1}$, thus $\sigma_{xx}(0) \propto \ln T$ [31]. The conductivity at zero field is plotted as a function of $\ln T$ in the inset of Fig. 4(b). Clearly below 20 K, $\sigma_{xx}(B=0)$ displays a linear dependence, characteristic of weak localization. Hence, at low temperatures, we observe the experimental evidence of weak localization in zero-field transport as well as the magnetotransport in our (Al, In)N/GaN system, both hallmarks of electron-electron scattering.

D. Angle dependence

To further investigate weak localization behavior, we vary the angle θ between the applied magnetic field and the c axis of crystal. Figure 5 shows the angle-dependent resistance at $T = 2$ K. At 0°, when the magnetic field is perpendicular to the sample, the magnetoresistance is pronounced and similar to the behavior described earlier. With the increase of the tilt angle, the influence of the magnetic field becomes smaller and weak localization is maintained over higher magnetic fields. At the highest tilt angle ($\theta = 88°$), the effects of weak localization dominate the entire field regime such that the resistance continues to decrease with the increasing magnetic field, displaying a negative magnetoresistance even up to 18 T. The crossover field where the magnetoresistance is lowest displays the anticipated linear dependence on $1/\cos\theta$. Furthermore, the SdH oscillations disappear gradually with increasing angle. If we plot the magnetoresistance as a function of the perpendicular component of the magnetic field $B\cos\theta$, the peaks collapse, respectively, for different angles, as shown in Fig. 5(b). Therefore, the behavior is controlled only by the perpendicular magnetic field, confirming the two-dimensional nature of electron transport in this heterostructure [7,14,15]. This is different from the orientation-insensitive behavior observed in three-dimensional nanostructures [20,32].

E. Discussion

As was discussed earlier, sample A with a carrier density $n_{\mathrm{SdH}} = 1.95\times10^{13}\,\mathrm{cm}^{-2}$ shows relatively small-amplitude Shubnikov–de Haas oscillations. In comparison, the second specimen sample B with approximately 20% lower carrier density $n_{\mathrm{SdH}} = 1.53\times10^{13}\,\mathrm{cm}^{-2}$, has longer lifetimes, higher mobility 2345 $\mathrm{cm}^2/\mathrm{V\,s}$, and a significantly larger SdH amplitude. An analysis of Eq. (3) shows that the inelastic scattering time in sample B is correspondingly bigger than that of sample A (Table I). Interestingly, even though in specimen B the quantum lifetime is twice that in sample A, it is also smaller than the transport lifetime and the ratio $\tau_t/\tau_q = 6.1$ (in sample B) is only slightly less than the ratio in sample A. Hence, at low temperatures small-angle scattering is the dominant scattering mechanism in

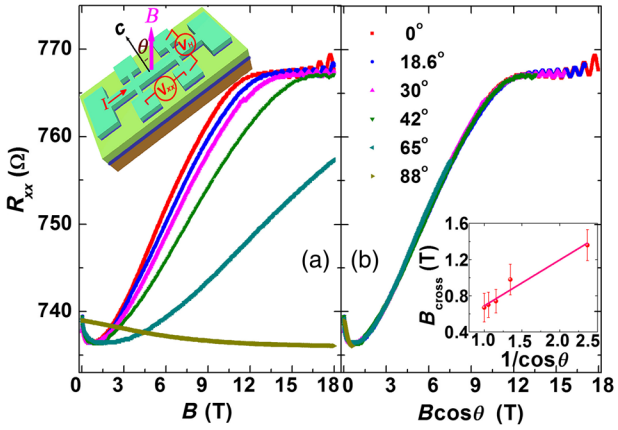

FIG. 5. (a) Angle dependence of the magnetoresistance at 2 K. (b) The magnetoresistance as a function of the perpendicular field, all data collapse to a single curve.

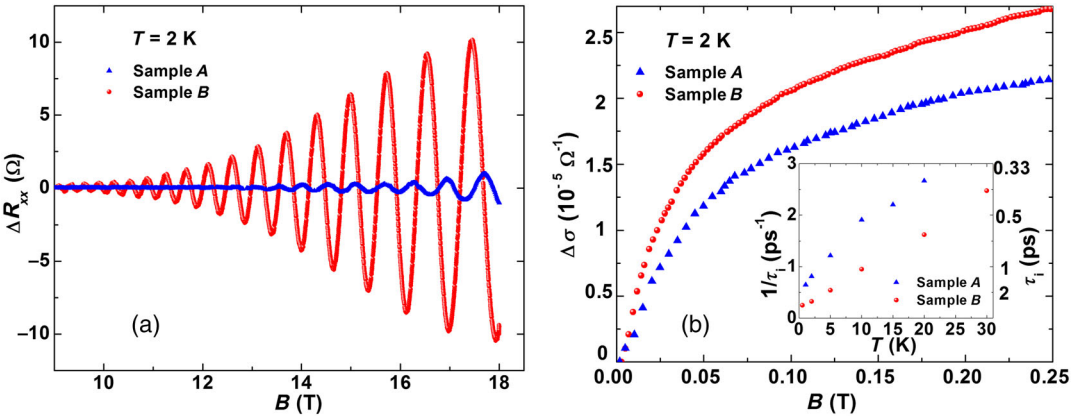

FIG. 6. (a) Shubnikov–de Haas oscillations for two samples. Clearly, sample *B* has stronger SdH oscillations. (b) Weak localization of two samples at 2 K. Inset is the inelastic relaxation time as a function of temperature.

both samples. But, as shown in Fig. 6(a), the maximum of ΔR_{xx} for sample *B* is around 10 Ω, one order of magnitude bigger than that of sample *A*. Not surprisingly, $\Delta\sigma$ due to weak localization in sample *B* is also larger than that in sample *A* [Fig. 6(b)]. That is, both types of quantum interferences are much stronger in the high-mobility and lower-density sample.

Table I lists the carrier density, quantum τ_q, transport τ_t, and inelastic (phase coherence) scattering (τ_i) time scales in related systems. For both samples *A* and *B*, due to strong small-angle scattering, quantum lifetime τ_q is the shortest, as a matter of fact about an order of magnitude smaller than τ_t. On the other hand, the inelastic time τ_i is the longest and much longer than both quantum and transport lifetimes. This same trend in time scales is also reported in $(\mathrm{Al,Ga})\mathrm{N/GaN}$ systems [25,33], as can be seen in Table I. Qualitatively, in a reduced Euclidean geometry, as in these 2DEG systems, the sensitivity to mean carrier-carrier separation, hence carrier density, is understandable. Also, the inelastic scattering rate is understandably smaller than the transport rate, which in turn is less than the quantum relaxation rate $((1/\tau_i) < (1/\tau_t) < (1/\tau_q))$.

Although both Shubnikov–de Haas and weak localization are quantum-mechanical phenomena, physically, the SdH effect is related to the momentum space (*k* space). It arises from the delicate tuning of the density of states as well as the Fermi level by the magnetic field. With increasing magnetic field, Landau levels periodically cross the Fermi level, resulting in oscillations of conductance. Whereas, weak localization is the nonclassical scattering of the carrier back to the origin due to constructive interference that requires robust phase memory, where small-angle scattering by long-range interaction is ineffective [11]. In other words, although small-angle scattering is frequent, only interactions that destroy phase coherence such as electron-electron and electron-phonon scatterings affect the weak localization process [34].

IV. CONCLUSION

The effect of scattering in 2DEG of $(\mathrm{Al,In})\mathrm{N/GaN}$ heterostructures has been studied through electrical transport and magnetotransport. Two dimensionality of the system is confirmed by angle-dependent measurement. A weak localization is observed in this material. We reason that the dominant phase-breaking mechanism is electron-electron scattering. Whereas in the Shubnikov–de Haas regime, we find that small-angle scattering is dominant. Furthermore, below 20 K the carrier mobility is slightly reduced with increasing temperature. In contrast, above 20 K the mobility rapidly decreases with increasing temperature as the scattering mechanism changes from acoustic phonons to optical phonons.

This study reaffirms the experience from the start of the semiconducting revolution, that device performance of all semiconducting systems including the new wide-band-gap heterostructures is critically influenced by the slightest differences in purity and processing. Furthermore, electron-electron scattering, small-angle scattering, acoustic phonons, and optical phonons all progressively contribute to

TABLE I. Comparison of Shubnikov–de Haas oscillation and weak localization parameters in GaN-based 2DEG at the lowest temperature, respectively.

System	Carrier density (10^{13} cm^{-2})	Quantum lifetime τ_q (ps)	Transport lifetime τ_t (ps)	Inelastic time τ_i (ps)
$Al_{0.83}In_{0.17}N/GaN$ (*A*)	1.95	0.035	0.25	1.66
$Al_{0.83}In_{0.17}N/GaN$ (*B*)	1.53	0.074	0.45	4.02
$Al_{0.25}Ga_{0.75}N/GaN$ (Ref. [25])	1.01	0.050	0.26	4.00
$Al_{0.22}Ga_{0.78}N/GaN$ (Ref. [33])	1.25	0.078	0.13	4.67

the decrease of mobility with rising temperature in the 2DEG of (Al, In)N/GaN heterostructures. An improved performance of high-power and high-frequency electronics using these materials can be achieved if unfavorable scatterings are reduced.

ACKNOWLEDGMENTS

We thank David Weber for the help with transport measurements, Ning Lu for the help in sample fabrication. The work is supported in part by DOE Award No. DE-NA0002630 and the University of South Carolina. A portion of this work was performed at the National High Magnetic Field Laboratory, which is supported by NSF Cooperative Agreement No. DMR-1157490 and the State of Florida.

[1] J. Kuzmik, Power electronics on InAlN/(In)GaN: Prospect for a record performance, IEEE Electron Device Lett. **22**, 510 (2001).

[2] R. Tülek, A. Ilgaz, S. Gökden, A. Teke, M. K. Öztürk, M. Kasap, S. Özçelik, E. Arslan, and E. Özbay, Comparison of the transport properties of high quality AlGaN/AlN/GaN and AlInN/AlN/GaN two-dimensional electron gas heterostructures, J. Appl. Phys. **105**, 013707 (2009).

[3] F. Wu, K. H. Gao, Z. Q. Li, T. Lin, and W. Z. Zhou, Effects of GaN interlayer on the transport properties of lattice-matched AlInN/AlN/GaN heterostructures, J. Appl. Phys. **117**, 155701 (2015).

[4] J. Kuzmik, G. Pozzovivo, C. Ostermaier, G. Strasser, D. Pogany, E. Gornik, J.-F. Carlin, M. Gonschorek, E. Feltin, and N. Grandjean, Analysis of degradation mechanisms in lattice-matched InAlN/GaN high-electron-mobility transistors, J. Appl. Phys. **106**, 124503 (2009).

[5] Z. J. Qiu, Y. S. Gui, T. Lin, N. Dai, J. H. Chu, N. Tang, J. Lu, and B. Shen, Weak localization and magnetointersubband scattering effects in an $Al_xGa_{1-x}N$/GaN two-dimensional electron gas, Phys. Rev. B **69**, 125335 (2004).

[6] F. V. Tikhonenko, D. W. Horsell, R. V. Gorbachev, and A. K. Savchenko, Weak Localization in Graphene Flakes, Phys. Rev. Lett. **100**, 056802 (2008).

[7] D. X. Qu, Y. S. Hor, J. Xiong, R. J. Cava, and N. P. Ong, Quantum oscillations and Hall anomaly of surface states in the topological insulator Bi_2Te_3, Science **329**, 821 (2010).

[8] M. B. Shalom, A. Ron, A. Palevski, and Y. Dagan, Shubnikov-De Haas Oscilltaions in $SrTiO_3/LaAlO_3$ Interface, Phys. Rev. Lett. **105**, 206401 (2010).

[9] Y.-W. Tan, J. Zhu, H. L. Stormer, L. N. Pfeiffer, K. W. Baldwin, and K. W. West, Measurements of the Density-Dependent Many-Body Electron Mass in Two Dimensional GaAs/AlGaAs Heterostructures, Phys. Rev. Lett. **94**, 016405 (2005).

[10] B. Grbic, R. Leturcq, T. Ihn, K. Ensslin, D. Reuter, and A. D. Wieck, Strong spin-orbit interactions and weak antilocalization in carbon-doped *p*-type GaAs/$Al_xGa_{1-x}As$ heterostructure, Phys. Rev. B **77**, 125312 (2008).

[11] S. McPhail, C. E. Yasin, A. R. Hamilton, M. Y. Simmons, E. H. Linfield, M. Pepper, and D. A. Ritchie, Weak localization in high-quality two-dimensional systems, Phys. Rev. B **70**, 245311 (2004).

[12] Y. Niimi, Y. Baines, T. Capron, D. Mailly, F.-Y. Lo, A. D. Wieck, T. Meunier, L. Saminadayar, and C. Bäuerle, Quantum coherence at low temperatures in mesoscopic systems: Effect of disorder, Phys. Rev. B **81**, 245306 (2010).

[13] N. Richter *et al.*, Robust Two-Dimensional Electronic Properties in Three-Dimensional Microstructures of Rotationally Stacked Turbostratic Graphene, Phys. Rev. Applied **7**, 024022 (2017).

[14] A. D. Caviglia, S. Gariglio, C. Cancellieri, B. Sacépé, A. Fête, N. Reyren, M. Gabay, A. F. Morpurgo, and J.-M. Triscone, Two-Dimensional Quantum Oscillations of the Conductance at $LaAlO_3/SrTiO_3$ Interfaces, Phys. Rev. Lett. **105**, 236802 (2010).

[15] H. Cao, J. Tian, I. Miotkowski, T. Shen, J. Hu, S. Qiao, and Y. P. Chen, Quantized Hall Effect and Shubnikov–de Hass Oscillations in Highly Doped Bi_2Se_3: Evidence for Layered Transport of Bulk Carriers, Phys. Rev. Lett. **108**, 216803 (2012).

[16] M. Lachab, M. Sultana, Q. Fareed, F. Husna, V. Adivarahan, and A. Khan, Transport properties of SiO_2/AlInN/AlN/GaN metal-oxide-semiconductor high electron mobility transistors on SiC substrate, J. Phys. D **47**, 135108 (2014).

[17] I. Gorczyca, T. Suski, N. E. Christensen, and A. Svane, Band gaps and built-in electric fields in InAlN/GaN short period superlattices: Comparison with (InAlGa)N quaternary alloys, Phys. Rev. B **93**, 165302 (2016).

[18] R. Butte *et al.*, Current status of AlInN layers lattice-matched to GaN for photonics and electronics, J. Phys. D **40**, 6328 (2007).

[19] E. A. Henriksen, S. Syed, Y. Ahmadian, M. J. Manfra, K. W. Baldwin, A. M. Sergent, R. J. Molnar, and H. L. Stormer, Acoustic phonon scattering in a low density, high mobility AlGaN/GaN field-effect transistor, Appl. Phys. Lett. **86**, 252108 (2005).

[20] L. Wang, M. Yin, J. Jaroszynski, and J.-H. Park, Geometric dependence of transport and universal behavior in three dimensional carbon nanostructures, Appl. Phys. Lett. **109**, 123104 (2016).

[21] S. B. Lisesivdin, A. Yildiz, N. Balkan, M. Kasap, S. Ozcelik, and E. Ozbay, Scattering analysis of two-dimensional electrons in AlGaN/GaN with bulk related parameters extracted by simple parallel conduction extraction method, J. Appl. Phys. **108**, 013712 (2010).

[22] Z. L. Miao *et al.*, Magnetotransport properties of lattice-matched $In_{0.18}Al_{0.82}N$/AlN/GaN heterostructures, J. Appl. Phys. **109**, 016102 (2011).

[23] A. Bayraklı, E. Arslan, T. Fırat, Ş. Özcan, Ö. Kazar, H. Çakmak, and E. Özbay, Magnetotransport study on AlInN/(GaN)/AlN/GaN heterostructures, Phys. Status Solidi A **209**, 1119 (2012).

[24] E. Frayssinet *et al.*, High electron mobility in AlGaN/GaN heterostructures grown on bulk GaN substrates, Appl. Phys. Lett. **77**, 2551 (2000).

[25] A. F. Braña, C. Diaz-Paniagua, F. Batallan, J. A. Garrido, E. Muñoz, and F. Omnes, Scattering times in AlGaN/GaN

two-dimensional electron gas from magnetoresistance measurements, J. Appl. Phys. **88**, 932 (2000).

[26] P. T. Coleridge, Small-angle scattering in two-dimensional electron gases, Phys. Rev. B **44**, 3793 (1991).

[27] M. J. Manfra, S. H. Simon, K. W. Baldwin, A. M. Sergent, K. W. West, R. J. Molnar, and J. Caissie, Quantum and transport lifetimes in a tunable low-density AlGaN/GaN two dimensional electron gas, Appl. Phys. Lett. **85**, 5278 (2004).

[28] R. G. Wheeler, Magnetoconductance and weak localization in silicon inversion layers, Phys. Rev. B **24**, 4645 (1981).

[29] S. Hikami, A. I. Larkin, and Y. Nagaoka, Spin-orbit interaction and magnetoresistance in the two dimensional random system, Prog. Theor. Phys. **63**, 707 (1980).

[30] K. K. Choi, D. C. Tsui, and K. Alavi, Dephasing time and one-dimensional localization of two-dimensional electrons in $GaAs/Al_xGa_{1-x}As$ heterostructures, Phys. Rev. B **36**, 7751 (1987).

[31] G. Du, V. N. Prigodin, A. Burns, J. Joo, C. S. Wang, and A. J. Epstein, Unusual semimetallic behavior of carbonized ion-implanted polymers, Phys. Rev. B **58**, 4485 (1998).

[32] L. Wang, M. Yin, M. Abdi, and T. Datta, Linear magnetoresistance in three-dimensional carbon nanostructure with periodic spherical voids, Appl. Phys. Lett. **107**, 023103 (2015).

[33] Z. J. Qiu, Y. S. Gui, T. Lin, J. Lu, N. Tang, B. Shen, N. Dai, and J. H. Chu, Scattering times in AlGaN/GaN two-dimensional electron gas from magnetotransport measurements, Solid State Commun. **131**, 37 (2004).

[34] D. Hoadley, P. McConville, and N. O. Birge, Experimental comparison of the phase-breaking lengths in weak localization and universal conductance fluctuations, Phys. Rev. B **60**, 5617 (1999).